Oral exposure to Ag or TiO2 nanoparticles perturbed gut transcriptome and microbiota in a mouse model of ulcerative colitis : Ag or TiO2 nanoparticles in ulcerative colitis

Wang, Shuyuan

2022-11

Wang , S , Kang , X , Alenius , H , Wong , S H , Karisola , P & El-Nezami , H 2022 , ' Oral exposure to Ag or TiO 2 nanoparticles perturbed gut transcriptome and microbiota in a mouse model of ulcerative colitis : Ag or TiO 2 nanoparticles in ulcerative colitis ' , Food and Chemical Toxicology , vol. 169 , 113368 . https://doi.org/10.1016/j.fct.2022.113368

http://hdl.handle.net/10138/354847
https://doi.org/10.1016/j.fct.2022.113368

Food and Chemical Toxicology 169 (2022) 113368

Contents lists available at ScienceDirect

Food and Chemical Toxicology

journal homepage: www.elsevier.com/locate/foodchemtox

Oral exposure to Ag or TiO_2 nanoparticles perturbed gut transcriptome and microbiota in a mouse model of ulcerative colitis

Shuyuan Wang [a], Xing Kang [b,c], Harri Alenius [d,e], Sunny Hei Wong [f], Piia Karisola [d,*], Hani El-Nezami [a,g]

[a] School of Biological Sciences, University of Hong Kong, Pokfulam Road, Hong Kong Special Administrative Region of China
[b] Department of Medicine and Therapeutics, The Chinese University of Hong Kong, Hong Kong Special Administrative Region of China
[c] State Key Laboratory of Digestive Disease, Institute of Digestive Disease, Li Ka Shing Institute of Health Sciences, The Chinese University of Hong Kong, Hong Kong Special Administrative Region of China
[d] Human Microbiome Research Program, University of Helsinki, Haartmaninkatu 3, 00290, Helsinki, Finland
[e] Institute of Environmental Medicine (IMM), Karolinska Institutet, Stockholm, 171 77, Sweden
[f] Lee Kong Chian School of Medicine, Nanyang Technological University, Singapore
[g] Nutrition and Health, Institute of Public Health and Clinical Nutrition, University of Eastern Finland, P.O. Box 1627, 70211, Kuopio, Finland

ARTICLE INFO

Handling Editor: Dr. Jose Luis Domingo

Keywords:
DSS-Induced colitis
Mouse model
Nanoparticles
Metal oxides
RSEQ
Inflammation
Gut microbiota
16S sequencing

ABSTRACT

Silver (nAg) and titanium dioxide ($nTiO_2$) nanoparticles improve texture, flavour or anti-microbial properties of various food products and packaging materials. Despite their increased oral exposure, their potential toxicities in the dysfunctional intestine are unclear. Here, the effects of ingested nAg or $nTiO_2$ on inflamed colon were revealed in a mouse model of chemical-induced acute ulcerative colitis. Mice (eight/group) were exposed to nAg or $nTiO_2$ by oral gavage for 10 consecutive days. We characterized disease phenotypes, histology, and alterations in colonic transcriptome (RNA sequencing) and gut microbiome (16S sequencing).

Oral exposure to nAg caused only minor changes in phenotypic hallmarks of colitic mice but induced extensive responses in gene expression enriching processes of apoptotic cell death and RNA metabolism. Instead, ingested $nTiO_2$ yielded shorter colon, aggravated epithelial hyperplasia and deeper infiltration of inflammatory cells. Both nanoparticles significantly changed the gut microbiota composition, resulting in loss of diversity and increase of potential pathobionts. They also increased colonic mucus and abundance of *Akkermansia muciniphila*. Overall, nAg and $nTiO_2$ induce dissimilar immunotoxicological changes at the molecular and microbiome level in the context of colon inflammation. The results provide valuable information for evaluation of utilizing metallic nanoparticles in food products for the vulnerable population.

1. Introduction

Ulcerative colitis (UC), a subtype of inflammatory bowel disease (IBD), is characterized by chronic inflammation starting at rectum and extending to parts of or entire colon. Fundamentally, IBD is the clinical manifestation of defective and uncontrolled gut immune responses to environmental triggers in genetically susceptible individuals. A precise understanding of what contributes to this immune malfunction remains unknown. The pathogenesis of IBD is multifaceted, as evidenced by data showing complicated interplay of inherent and external factors such as genetics, diet, and stress (Maloy and Powrie, 2011). The dysfunction of intestinal epithelial barrier has been identified to play a key role in UC pathogenesis. These patients have a so-called "leaky" gut due to disrupted tight junction proteins between the epithelial cells and reduced mucus barrier. As a result, there is enhanced penetration of inflammogenic luminal matters (bacteria or food antigens) into the mucosal layer, causing local inflammation (Söderholm et al., 2002; Edelblum and Turner, 2009).

An increasing body of evidence suggests that gut dysbiosis at the mucosal front plays a critical role in development of relapsing IBD (Nagao-Kitamoto et al., 2016; Duboc et al., 2013; Panpetch et al., 2020; Rajca et al., 2014; Seekatz et al., 2014; Ni et al., 2017). Patients are associated with an increased population of pro-inflammatory Proteobacteria members such as *Enterobacteriaceae*(Seksik et al., 2003;

* Corresponding author.
E-mail addresses: wangsy@connect.hku.hk (S. Wang), jason.kangxing@link.cuhk.edu.hk (X. Kang), harri.alenius@helsinki.fi (H. Alenius), sunny.wong@ntu.edu.sg (S.H. Wong), piia.karisola@helsinki.fi (P. Karisola), elnezami@hku.hk (H. El-Nezami).

https://doi.org/10.1016/j.fct.2022.113368
Received 11 May 2022; Received in revised form 5 August 2022; Accepted 10 August 2022
Available online 7 September 2022

Baumgart et al., 2007) and a lower amount of anti-inflammatory Firmicutes bacteria, specifically *Faecalibacterium prausnitzii* (Manichanh et al., 2006; Walker et al., 2011; Frank et al., 2007; Halfvarson et al., 2017). With an overgrowth of pathogenic species and a breach in barrier integrity, pathogen-associated molecular patterns (PAMPs) on bacteria readily bind to pattern recognition receptors (PRRs) such as Toll-like receptors (TLRs) on intestinal epithelial cells or immune cells, activating a cascade of inflammatory responses and immunetoxicity (Ni et al., 2017). However, a causal relationship between gut dysbiosis and IBD development cannot be definitively elucidated since it remains unclear if the former precedes or results from existing inflammation (Ni et al., 2017).

Food additives, such as titanium dioxide (TiO_2) and silver (Ag), have been abundantly used in modern food products and western diet. However, European Union member states decided to ban the use of TiO_2 as E171 food additive in early 2022, due to a lack of definite conclusion in its safety assessment (European Commission, 2021). Nanosized TiO_2 ($nTiO_2$) particles contribute up to 36% of the food whitening agent E171 (Weir et al., 2012; Peters et al., 2014). Nanosized silver (nAg) particles also present in a considerate amount (23%) in food coloring additive E174(Waegeneers et al., 2019), in addition to their wide use in food packaging materials to eliminate odors and extend shelf-life. Both $nTiO_2$ and nAg are popular food additive components that are present in assorted food types including coffee creamer, chewing gums, cakes, chocolates, confectionary sweets (Chaudhry et al., 2008; Srinivas et al., 2010), which gives rise to increased oral exposure to these nanoparticles in the general population.

Metal-type nanoparticles are known for their anti-microbial properties. While both nAg and $nTiO_2$ have been shown to induce mild to major microbial alterations in gut of healthy or obese mice(Van Den Brûle et al., 2015; Williams et al., 2015; Pinget et al., 2019; Cao et al., 2020), their impact on the gut microbiota in UC is less known. Several studies have shown that $nTiO_2$ particles were found present in the Peyer's patches and blood samples of IBD patients (Ruiz et al., 2017; Lomer et al., 2002, 2004). Owning to a close link between medical conditions such as IBD and a disrupted gut microbiota, it is important to examine whether nAg or $nTiO_2$ influences the commensal gut flora in colitis mice. Our study aimed to assess the biological effects and potential immunotoxicity of oral exposure to nAg or $nTiO_2$ on gut gene expression and microbiota in a mouse model of dextran sulphate sodium (DSS)-induced colitis. A transcriptomic approach was taken for this study to reveal the global transcriptional alterations induced by the tested particles. This approach captures comprehensive changes that are partly missing in conventional assays such as real-time PCR and measurement of inflammatory markers in tissue or serum.

2. Materials and methods

2.1. Nanoparticles and suspension preparation

Nanoscale pre-made dispersion (5 mg/ml) of Ag and powered TiO_2 were purchased from NanoComposix (San Diego, United States) and Nanostructured & Amorphous Materials, Inc. (Houston, United States) respectively. Properties of these nanoparticles provided by the manufacturers are summarized in Table 1. A detailed characterization of the same materials has been performed and published previously (Poon et al., 2017). TiO_2 suspensions were prepared freshly on each treatment day by dispersing the powders in autoclaved MilliQ water (vehicle in this experiment), followed by 30-s vortexing and 20-min water-bath sonication at 30 °C. Both Ag and TiO_2 dispersions were vortexed for 30 s immediately before oral gavage.

Table 1
Nanoparticle intrinsic characteristics provided by the manufacturers.

	nAg	$nTiO_2$
Size	25 nm	30–40 nm
Form	Dispersion in H_2O	Powders
Composition	–	Anatase/rutile: 90:10
Specific surface area	21.1 m^2/g	30 m^2/g
Purity	99%	99%
Coating	Polyvinylpyrrolidone (PVP)	–

2.2. Mice

All animal procedures were approved by Committee on the Use of Live Animals in Teaching and Research, University of Hong Kong. After one-week acclimatization, male C57BL/6J mice aged six to seven weeks were caged in groups of three to four in individually ventilated cages and were provided with standard chow diet and autoclaved tap water *ad libitum* when not receiving any treatment. A carefully controlled animal environment with a 12-h light-dark cycle at 22 °C was provided for the mice.

2.3. Animal treatment protocol

Mice (eight per group) were randomly assigned to one of the following groups: DSS and vehicle (DSS + Veh); DSS and nAg (DSS + Ag); DSS and $nTiO_2$ (DSS + TiO_2) (Fig. S1A). Additional groups of healthy control mice (Naïve) and mice receiving DSS alone (DSS) were also included (data shown in supplementary document), with eight mice per group. Two-percent (wt/vol) DSS (molecular weight, 36,000–50,000; MP Biomedicals) dissolved in sterile drinking water was provided to the mice *ad libitum* for seven days to induce colitis, followed by a recovery period (switched to normal drinking water) of three days. Throughout the 10 days, autoclaved water (vehicle), 50 mg/kg Ag or 500 mg/kg TiO_2 suspensions were administered via oral gavage. Immediate oral gavage after sonication and vortexing was chosen as the route of exposure to deliver a precise dose of particles and to avoid particle aggregation that would otherwise happen when left in food or drinking water over time. Mice were sacrificed by overdose of sodium pentobarbitone. Colon tissue was harvested and stored in RNAlater® solution (Life Technologies Ltd., Paisley, UK) or fixed in formalin for further analysis. One fecal pellet expelled from each mouse was collected in an empty and sterilized cage, as described by Langille et al. (2014) Fecal samples were stored at −80 °C immediately after collection until microbiome analysis.

2.4. Dose selection

Different concentrations have been studied and tested in previous publications, ranging from 1 mg/kg to 1 g/kg for nAg(Williams et al., 2015; van der Zande et al., 2012; Shahare et al., 2013; Wilding et al., 2016; Park et al., 2010), and from 2.5 mg/kg to 5 g/kg for $nTiO_2$ (Ruiz et al., 2017; Gao et al., 2021; Bettini et al., 2017; Wang et al., 2007a, 2013; Zhao et al., 2013). Our doses were selected based on the limited data on human real-life exposure and likely underestimation due to the rather loose or even absent restrictions on the use of nAg or $nTiO_2$ in food products in EU (before 2022) and United States (Medina-Reyes et al., 2020). The estimated dietary intake of Ag and TiO_2 range from 1.29 μg/kg/day to 6.59 μg/kg/day and 1 mg/kg/day to 3 mg/kg/day respectively(Weir et al., 2012; EFSA Panel on Food Additives, 2016), depending on age groups, consumers' locations and dietary habits. In USA, the FDA-approved maximum use of E171 is 1% of the final weight of the food product (United States Food and Drug Administration, 2017). Based on the previous report that 36% of the particles in E171 fall within the nanoscale (Weir et al., 2012), the daily oral exposure to $nTiO_2$ was estimated to be 4000 mg × 1% x 36% = 14.4 mg/mouse (corresponding to [weight of food] x [maximum amount of E171] x [proportion of $nTiO_2$]), i.e. 720 mg/kg (assume a 20 g mouse eats 4 g food per day), and thus 500 mg/kg was selected as the dose of $nTiO_2$ in this study. A lower dose of nAg, 50 mg/kg, was chosen due to its expected lower human

exposure level compared to $nTiO_2$ (EFSA Panel on Food Additives, 2016).

2.5. Macroscopic evaluation of colitis

On each experimental day, body weights of mice were measured and stool samples were collected and tested for presence of occult fecal blood using Hemoccult® Sensa® Single Slides Rapid Diagnostic Test Kit (Beckman-Coulter, CA, United States) according to the manufacturer's protocol. Disease activity index (DAI), a sum of marks for body weight loss, stool consistency, and presence of fecal blood, was calculated based on a scheme shown in Table 2 (Murano et al., 2000). On sacrifice day, the entire colon was excised and its length was measured.

2.6. Histological assessment

In the histological analysis, 1 cm of colon was fixed in 10% buffered formalin and embedded in paraffin and then 4-μm colon sections were cut and stained with hematoxylin and eosin (H&E) to score: (Erben et al., 2014): the depth of inflammation (0, absence of infiltrate; 1, infiltrate found at the mucosa; 2, infiltrate reaches the submucosa; 3, infiltrate involves the muscularis propria), the degree of epithelial hyperplasia (0, none; 1, mild; 2, moderate; 3, severe), and the extent of epithelial erosion (0, none; 1, focal, < 20% of total mucosa; 2, small, 20–40% of total mucosa; 3, large, >40% of total mucosa). An overall score of histological damage was obtained by taking the average of the three scores, where inflammation weighs 50% while hyperplasia and erosion weigh 25% each. Periodic acid Schiff-Alcian blue (PAS-AB) stain (Thermo Fisher Scientific, United States) was used to examine changes in mucus quantity, following the manufacturer's protocol. Acidic, neutral and mixed mucosubstances were stained as blue, magenta and bluish purple respectively. The specific and total stained area was determined by color-thresholding in ImageJ and was divided by the total length of mucosa, to give stain density of mucosubstances (Amat et al., 2017; Zhu et al., 2015; Livraghi et al., 2009).

2.7. Colon RNA extraction and transcriptomics analysis

Colon samples were homogenized in lysis buffer and extracted using RNeasy® Plus Mini kit (Qiagen) according to the manufacturer's protocol. The concentration and integrity of isolated RNA was measured by NanoDrop spectrophotometer (ND-1000, Thermo Fisher Scientific Inc., United States). Library preparation was carried out using the Nextera XT DNA sample prep kit (Illumina, United States) according to manufacturer's instruction. The 3'end-amplified fragments were sequenced on the Illumina NextSeq 500 platform. RNA sequencing was conducted based on the Drop-seq protocol and the reads were processed following the pipeline adopted by Macosko et al. (2015) The sequenced reads were filtered and trimmed to less than 20 nt via the tool Trimmomatic (parameters: LEADING:3, TRAILING:3, SLIDINGWINDOW:4:15 and MINLEN:36). PolyA tails of length six or greater was further removed in the Drop-seq tools (https://github.com/broadinstitute/Drop-seq). Thereafter the processed reads were mapped to GRCm38.p6 whole genome using STAR (v2.6.0a) with the default settings for gene annotation. Raw read counts were calculated using featureCounts software (v1.6.4). Gene counts between the samples were Trimmed Mean of the M values (TMM) normalized and differential gene expression analysis was conducted in a negative binomial linear model and Wald tests with low expression outliers removed using Cook's distance in edgeR. The threshold for significance was set at fold change greater than |1.25| and Benjamini Hochberg adjusted $p < 0.05$.

The identified differentially expressed genes (DEGs) were hierarchically clustered in the software Perseus based on the Euclidean method and the k-means algorithm, based on Z-score normalized log2-transformed gene expression intensity values of the 23 DEGs that were tested ANOVA-positive ($p \leq 0.05$) in Perseus (Tyanova et al., 2016). Principle component analysis (PCA) plot was also established in Perseus, computed based on the log2-transformed read counts of total DEGs between different treatment groups. Venn diagrams were created in Venny 2.1.0 to indicate the distribution of DEGs between sample groups (OliverosVenny, 2007). Gene enrichment analysis was performed in PANTHER to reveal the GO biological processes induced by the DEGs (Mi et al., 2017). In addition, Diseases or Functions Annotation analyses were performed in Ingenuity Pathway Analysis (IPA) software (Qiagen, United States) to elucidate the downstream outcome of up- or down-regulated DEGs when comparing nanoparticle-treated groups (Ag or TiO_2) with vehicle control group (Krämer et al., 2014), with a cut-off for significantly enriched annotation set at adjusted $p < 0.05$ and the exclusion of "cancer" category.

2.8. 16S sequencing and analysis

DNA was extracted from mice fecal samples using QIAamp® PowerFecal® Pro DNA Kit (Qiagen, Germany) according to the manufacturer's protocol. The V3–V4 hypervariable region was amplified with Phusion® High-Fidelity PCR Master Mix (New England Biolabs, United States), and assessed for purity and integrity by 5400 Fragment Analyzer system (Agilent). The PCR product was then extracted by Qiagen Gel Extraction Kit (Qiagen, Germany) according to the manufacturer's protocol. Thereafter the samples were quantified via Qubit 2.0 Fluorometer (Thermo Scientific, United States) and prepared for sequencing using the NEB Next Ultra DNA library prep kit (New England Biolabs, United States).

16S sequencing was performed on an Illumina NovaSeq 6000 sequencing platform generating 250-bp paired-end reads (Novogene Bioinformatics Technology Co., Ltd.). The raw reads were overlapped by linking them from each sample using FLASH (Version 1.2.10) with default parameters (Magoč and Salzberg, 2011). Raw tags were truncated from continuous low-quality base site (default quality threshold ≤19) to the first low-quality base point that reaches the set length (default length value 3), and sequences with continuous high-quality bases of less than 75% of tag length were also filtered to obtain high quality clean tags in QIIME (Version 1.7.0) (Caporaso et al., 2010; Bokulich et al., 2013). After the filtering, chimeric sequences were detected and removed using UCHIME algorithm against the reference database (Gold) to obtain Effective Tags that were used to match Operational Taxonomy Units (OTUs) (Edgar et al., 2011). OTUs were assigned to each sample based on 97% similarity threshold in UPARSE software (Version 7.0.1001) (Edgar, 2013). Taxonomic annotations were given with reference to the SILVA database in MOTHUR (Wang et al., 2007b; Quast et al., 2012). The alpha (within-sample) diversity was estimated by Shannon and Simpson indices in QIIME. Furthermore, based on the relative abundance matrix, linear discriminant analysis effect size analysis (LEfSe) was conducted in LEfSe software to indicate the between-sample differences with regard to the most differentially abundant taxa, with a threshold for Linear discriminant analysis (LDA) score set at 4.

2.9. Statistical analysis

All data are presented as means ± standard error (SEM), unless otherwise stated specifically in the figure legend. The differences

Table 2
Parameters and scoring scheme for DAI.

Score	Body weight loss (%)	Stool consistency	Blood in stool
0	<1	Well-formed pellets	Absence
1	1–5	Soft still formed	Trace blood
2	6–10	Soft	Mild hemoccult
3	11–15	Very soft	Obvious hemoccult
4	>15	Watery/Diarrhea	Gross bleeding

between groups were analyzed in GraphPad Prism 6 software (GraphPad Software, Inc. San Diego, CA) using non-parametric Mann–Whitney *U* test, unless otherwise specified. *p < 0.05; **p < 0.01; ***p < 0.001; and ****p < 0.0001.

3. Results

3.1. nAg did not affect disease phenotypes while nTiO$_2$ shortened colon length

We used murine model of DSS-induced colitis to mimic human ulcerative colitis (Fig. S1A), a type of colon inflammation afflicting millions of people worldwide. A direct injury to colonic cells was induced in mice by DSS molecules dissolved in drinking water. We first sought to examine the macroscopic changes that occurred over the 10-day experimental period. Mice that had received DSS started to lose weight on day 5 compared to the naïve mice. NAg-exposed mice were slightly heavier compared to the vehicle control on days 9 and 10, although no significant difference was noted between them (Fig. S1B). In addition, the body weight of DSS-treated alone mice (no gavage) dwindled significantly as opposed to naïve mice (Fig. S2A). Fig. S1C and Fig. S2B reveal DSS-treated mice showed significantly higher DAI values

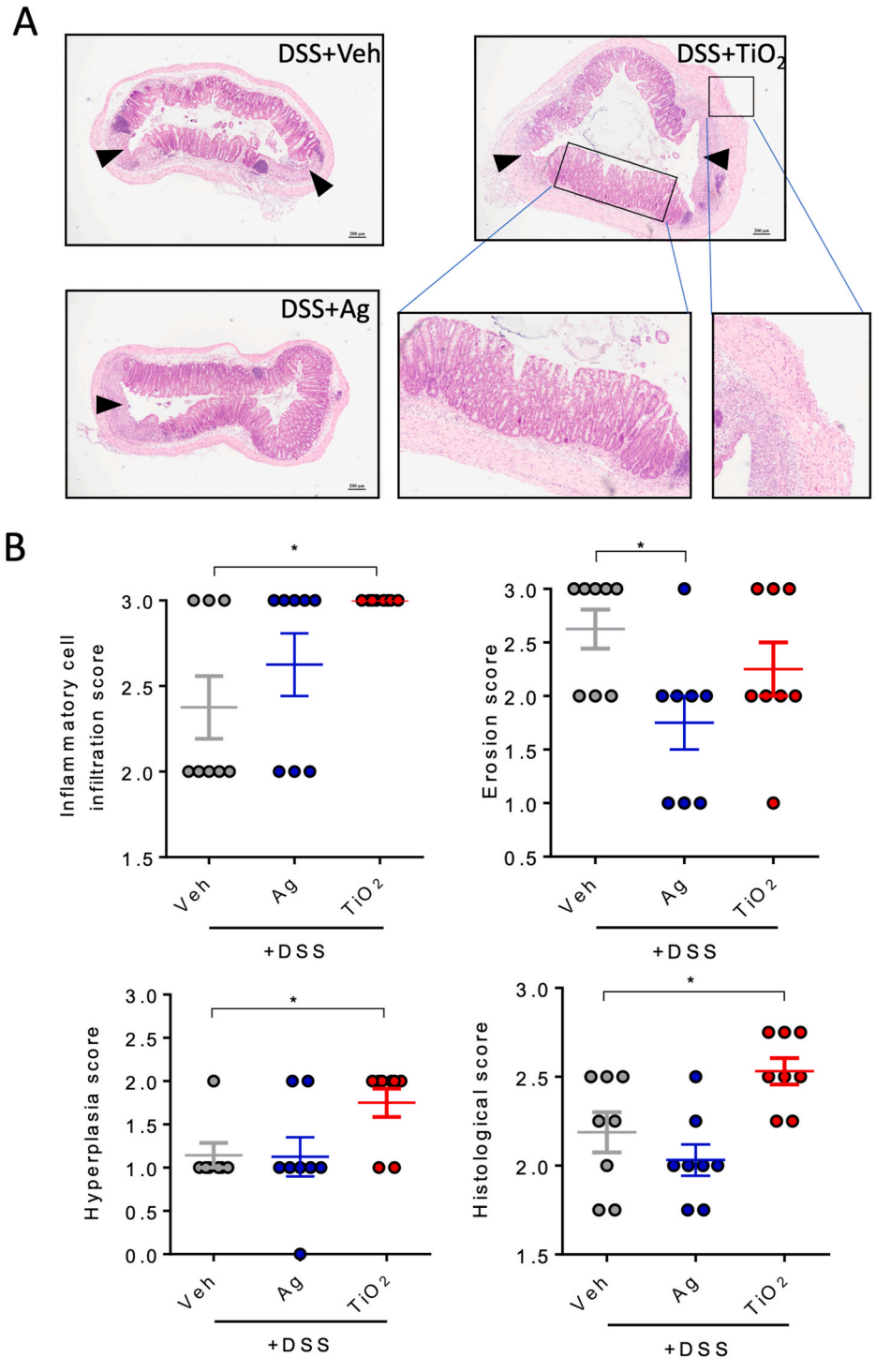

Fig. 1. Effect of Ag and TiO$_2$ nanoparticles on histopathological changes of colon. (A) Representative pictures of H&E-stained colon tissue from each group taken at 40x magnification are shown. Arrowheads indicate the eroded area of mucosal layer. (B) Scores of depth of inflammatory cell infiltration, hyperplasia, erosion and a weighted average of overall histological damage (inflammation: 50% weighting; hyperplasia and erosion: 25% weighting each) are shown. Data are represented as means ± SEM in B. Differences between the groups (N = 8/group) were studied by Mann–Whitney *U* test, *p < 0.05.

compared to the naïve mice. There was no statistically significant difference between nAg- or $nTiO_2$-fed mice versus the vehicle control (Fig. S1C). Colon shortening is another macroscopic feature that prevails in DSS-induced colitis mice model. DSS-treated mice had significantly shorter colon than the naïve mice (Fig. S1D and Fig. S2C). While nAg did not change colon length, $nTiO_2$ further shortened the colon compared to vehicle treatment (Fig. S1D).

3.2. *Histological hallmarks altered by nAg or $nTiO_2$ in colitis mice*

We next sought to evaluate the potential differences in histological manifestations of inflamed colon tissue with or without the exposure to nAg or $nTiO_2$. DSS treatment significantly damaged the normal colon histology (Fig. S2D). Representative H&E-stained colon pictures from vehicle, nAg- or $nTiO_2$-exposed mice are provided in Fig. 1A. The score on inflammatory cell infiltration was greater in $nTiO_2$ group compared to the vehicle group, indicating a deeper degree of penetration of immune cells reaching the colon muscularis layer (Fig. 1B). Epithelial hyperplasia was also more severe in mice exposed to $nTiO_2$ (Fig. 1B). On the other hand, nAg treatment reduced the area of eroded colon compared to the vehicle (Fig. 1B). Overall, ingestion of $nTiO_2$ induced greater damages to the mouse colon based on the histological evaluation while nAg did not cause significant harm (Fig. 1B).

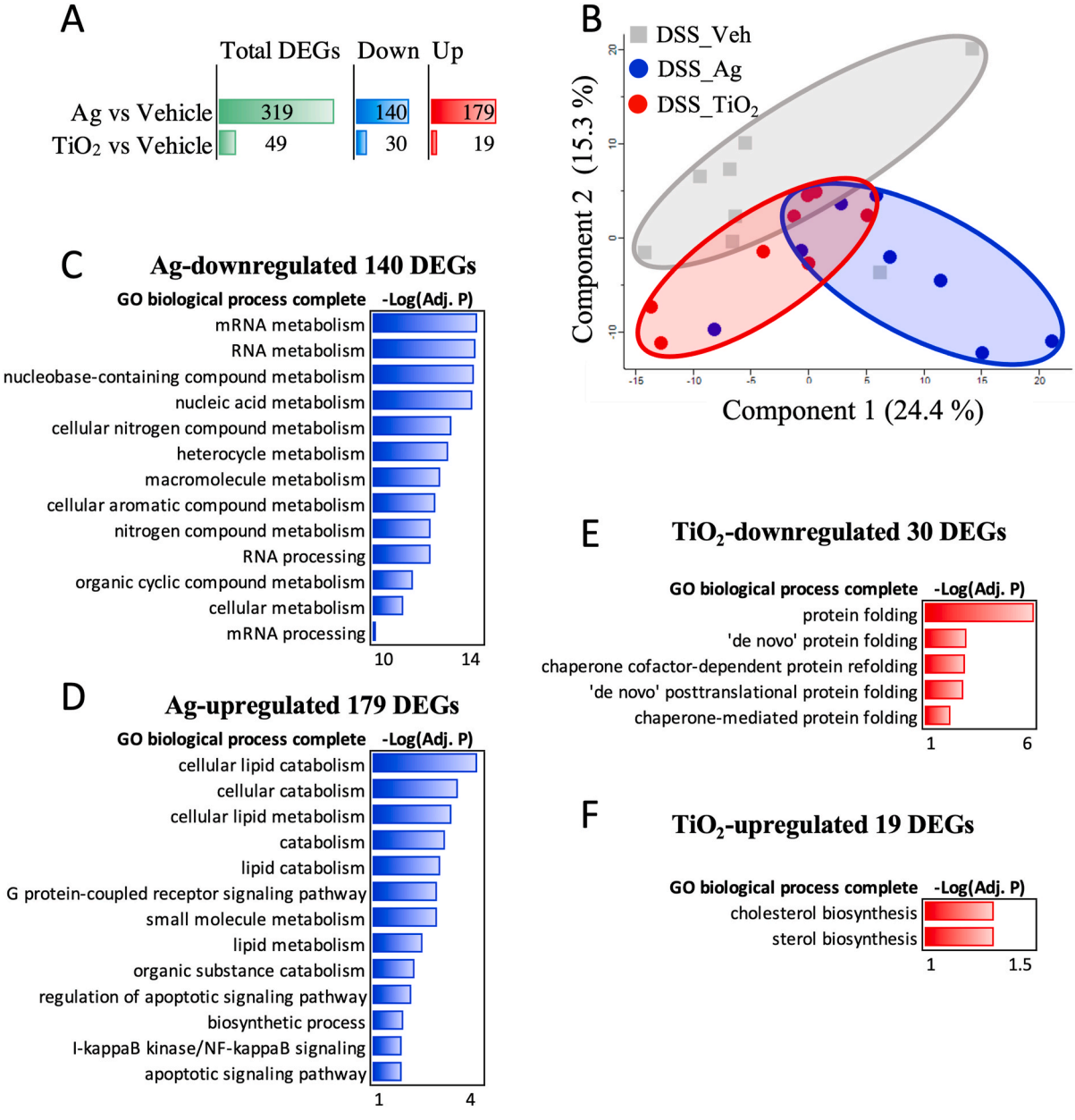

Fig. 2. Differentially expressed genes (DEGs). Principal component analysis (PCA) of TMM-normalized gene expression of ENM-exposed and control gut samples. (A) Ag or TiO_2 in vehicle induced varying numbers of differentially expressed genes (DEGs, $P < 0.05$ and $FC>|1.25|$) in the mouse colon at day 10 ($N = 8$/group). Total number of DEGs, and up- and downregulated DEGs are shown. (B) PCA shows the clustering of the samples of DSS-Vehicle (grey filled squares), TiO_2 (red circles) and Ag (blue circles). Principal components are based on the 327 DEGs, and components 1 and 2 are shown. The biological processes of Ag-induced downregulated DEGs (C) and upregulated DEGs (D), and TiO_2-induced downregulated DEGs (E) and upregulated DEGs (F) on Panther gene ontology database and associated negative log-transformed p-values with Benjamini-Hochberg correction for multiple testing are shown. (For interpretation of the references to color in this figure legend, the reader is referred to the Web version of this article.)

3.3. nAg held a greater potential in triggering changes in colonic transcriptome

To identify the nAg- or $nTiO_2$-driven transcriptional changes, we studied genome-wide gene expression from mouse colon by next-generation sequencing after 10-day consecutive oral exposure. It was shown that total 327 differentially expressed genes (DEGs) were induced by nAg or $nTiO_2$ particles compared to the vehicle treatment. Ingestion of nAg elicited more alterations in gene expression pattern than $nTiO_2$, inducing 319 DEGs. In stark contrast, only 49 DEGs were triggered as a consequence of $nTiO_2$ exposure (Fig. 2A). DEG analysis also reveals that DSS-treated mice had 1393 DEGs in total (where 1334 DEGs were unique) compared to the naïve mice (Figs. S3A–B), verifying the distinct gene expression pattern induced by DSS treatment. In PCA analysis based on total 327 DEGs, the three distinct clusters also indicate differences in gene expression pattern between the different treatments (Fig. 2B). The identified DEGs for each comparison were matched with their significantly associated GO biological processes in PANTHER (Mi et al., 2017). DSS treatment alone compared to the naïve condition caused significant perturbations in cell metabolism and biological

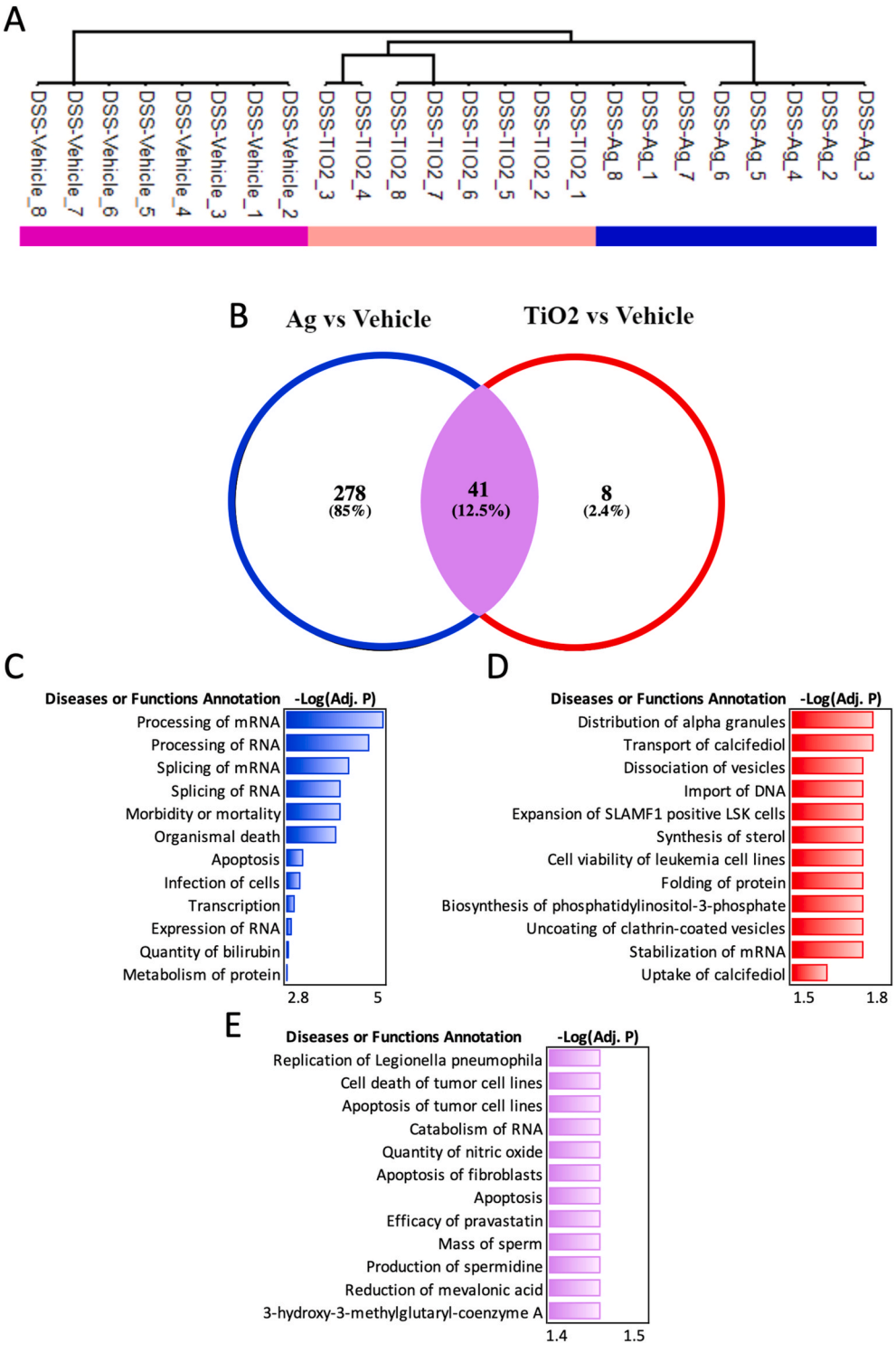

Fig. 3. Differential gene expression analysis. (A) Hierarchical clustering of Z-score normalized log2-transformed intensity values of the top 23 DEGs (ANOVA-positive at $p \leq 0.05$) at day 10 using Perseus software tool is shown. (B) Venn diagram shows the number of DEGs (post hoc adj. $p < 0.05$, linear FC>|1.25|) in colon of nanoparticle-treated mice (50 and 500 mg/kg for Ag and TiO_2 respectively, N = 8/group). Diseases and Functions (cancer excluded) that were specifically enriched by DEGs from (C) Ag, (D) TiO_2 exposure, and (E) commonly enriched by shared DEGs between Ag and TiO_2 when compared with vehicle control, and associated Benjamini-Hochberg corrected –log p-values are shown in a bar graph.

regulation processes, likely mediated via MAPK signalling pathway (Fig. S3C). Gene enrichment analysis reveals that DEGs of nAg led to more significantly enriched biological processes while the smaller number of $nTiO_2$-associated DEGs enriched much fewer events (Fig. 2C–F). Metabolism of RNA, cellular nitrogen compounds, and mRNA processing activities were highly enriched by nAg-induced downregulated DEGs (Fig. 2C). Additionally, nAg induced upregulation of DEGs that participated in lipid catabolism processes. To a lesser extent, nAg-associated DEGs also enriched events of apoptotic and I-κB kinase/NF-κB signaling (Fig. 2D). $NTiO_2$ exposure, on the other hand, most significantly downregulated DEGs related to protein folding processes (Fig. 2E–F).

3.4. Modulatory effects of ingested nAg or nTiO2 on biological functions

In line with the PCA analysis, hierarchical clustering shows that nAg and $nTiO_2$ altered colonic transcriptome in colitis mice (Fig. 3A). To shed more light on the biological significance of treatment-specific DEGs, we conducted Venn analysis to investigate the exclusive sets of DEGs in comparisons between each nanoparticle-treated group against the vehicle control, and the shared set of DEGs. The largest number of DEGs (278) was shown to be specific to nAg-treated mice, contributing to 85% of total DEGs. On the contrary, $nTiO_2$ did not trigger major specific changes at the transcriptional level, inducing only 8 (2.4%) exclusive DEGs. In addition, 41 DEGs (12.5%) were shared between responses induced by the two types of nanoparticles compared to the vehicle mice (Fig. 3B). Next, we assessed the biological implications of both exclusive and common sets of DEGs by Disease or Function analysis in IPA. Exposure to nAg led to DEGs that contributed to processing and splicing of mRNA and RNA, apoptosis, infection of cells and transcription (Fig. 3C). For TiO_2-specific DEGs, they were mainly associated with protein folding and biosynthesis of phosphatidylinositol 3-phosphate (Fig. 3D). The shared set of DEGs slightly enriched responses such as cell death, apoptosis, and catabolism of RNA (Fig. 3E).

3.5. nAg and $nTiO_2$ perturbed the composition of gut microbiota in colitis mice

In addition to the transcriptional changes, 16S rRNA sequencing of fecal samples was conducted to examine whether oral exposure to nAg

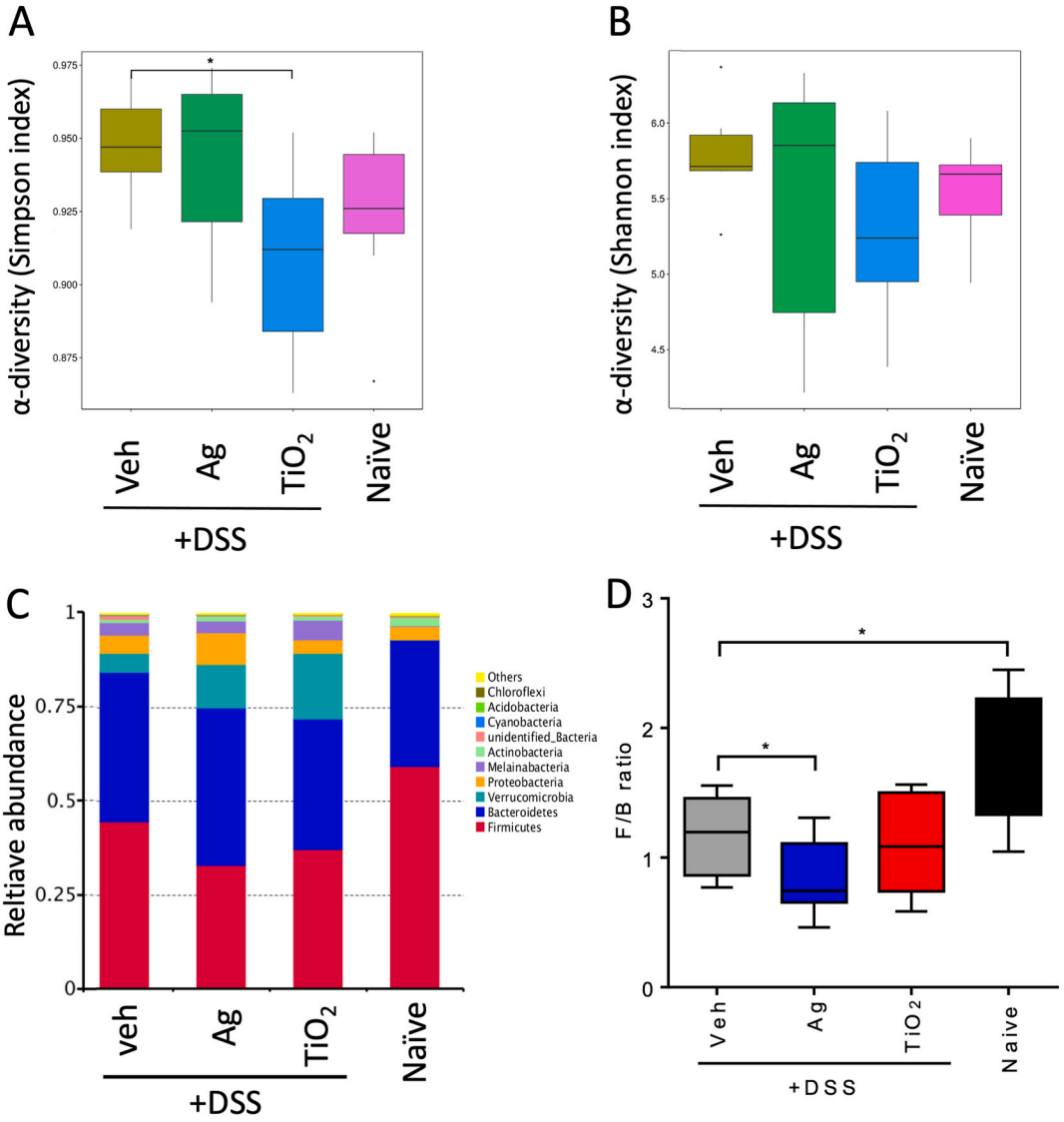

Fig. 4. Ag and TiO_2 nanoparticles altered the composition of gut microbiota. Fecal pellets collected on day 10 were analyzed for gut microbiome by 16S rRNA sequencing. (A–B) α-diversity is shown by Simpson and Shannon indices, and (C) relative abundance of total ten OTUs in stool samples is shown after different treatments. Phylum-level taxonomies are presented as a percentage of total sequences. (D) Firmicutes to Bacteroidetes (F/B) ratio of the gut microbiota is based on relative abundance. Data in A, B and D represent min, mean, max. Differences between the groups (N = 8/group) were studied by Mann–Whitney *U* test, *p < 0.05.

or $nTiO_2$ modulated the composition of gut microbiota in DSS-colitis mice. Fig. 4A–B indicate the α-diversity of different groups measured by Simpson and Shannon indices respectively. Mice administered with $nTiO_2$ showed a significantly lower Simpson index compared to vehicle control (Fig. 4A). A similar observation was also seen in Shannon index, although not reaching statistical significance (Fig. 4B). Further analysis at the phylum level showed that both nAg and $nTiO_2$ treatments notably modified the gut microbial profiles, compared with the vehicle control. Particularly, nAg was able to enhance the abundance of Bacteroidetes and Proteobacteria while $nTiO_2$ boosted the growth of Verrucomicrobia and Melainabacteria (Fig. 4C). Furthermore, the Firmicutes to Bacteroidetes (F/B) ratio in mice treated with nAg was significantly lower than the vehicle control, while this ratio was the highest in healthy mice (Fig. 4D).

Next, heat map analysis was conducted to reveal compositional differences induced by oral intakes of nAg or $nTiO_2$ in DSS-colitis mice at the genus level (Fig. 5A). It was clear that naïve mice had a distinct profile of gut flora from the other DSS-treated groups. For example, the abundance of *Bifidobacterium* was more abundant in naïve mice. A number of particle-specific alterations in the relative abundance of gut microbiota were seen at the genus level. *Bacteroides*, *Enterococcus* and genus from *Enterobacteriaceae* were increased in nAg-treated mice. Populations of *Romboutsia*, *Turicibacter*, *Akkermansia* and genus from *Ruminococcaceae* were seen enriched after $nTiO_2$ exposure (Fig. 5A). A Cladogram after LEfSe analysis demonstrates that the populations of the class Gammaproteobacteria, the order Enterobacteriales and the family *Enterobacteriaceae* (all belonging to the phylum Proteobacteria) were enhanced distinctively in nAg-fed mice when compared with vehicle- and $nTiO_2$-dosed mice. On the other hand, a pronounced increase in abundance of bacteria from the phylum Verrucomicrobia was noticed in $nTiO_2$-treated mice (Fig. 5B).

3.6. Nanoparticles increased colonic mucus and Akkermansia muciniphila

The relative population of *Akkermansia* spp. was elevated in DSS-treated mice when compared to the naïve mice (Fig. 6A). Both nAg and $nTiO_2$ mice showed higher relative abundance of *Akkermansia muciniphila* than the vehicle mice (Fig. 6B). The genus *Akkermansia* has been associated with maintaining colonic mucus homeostasis and

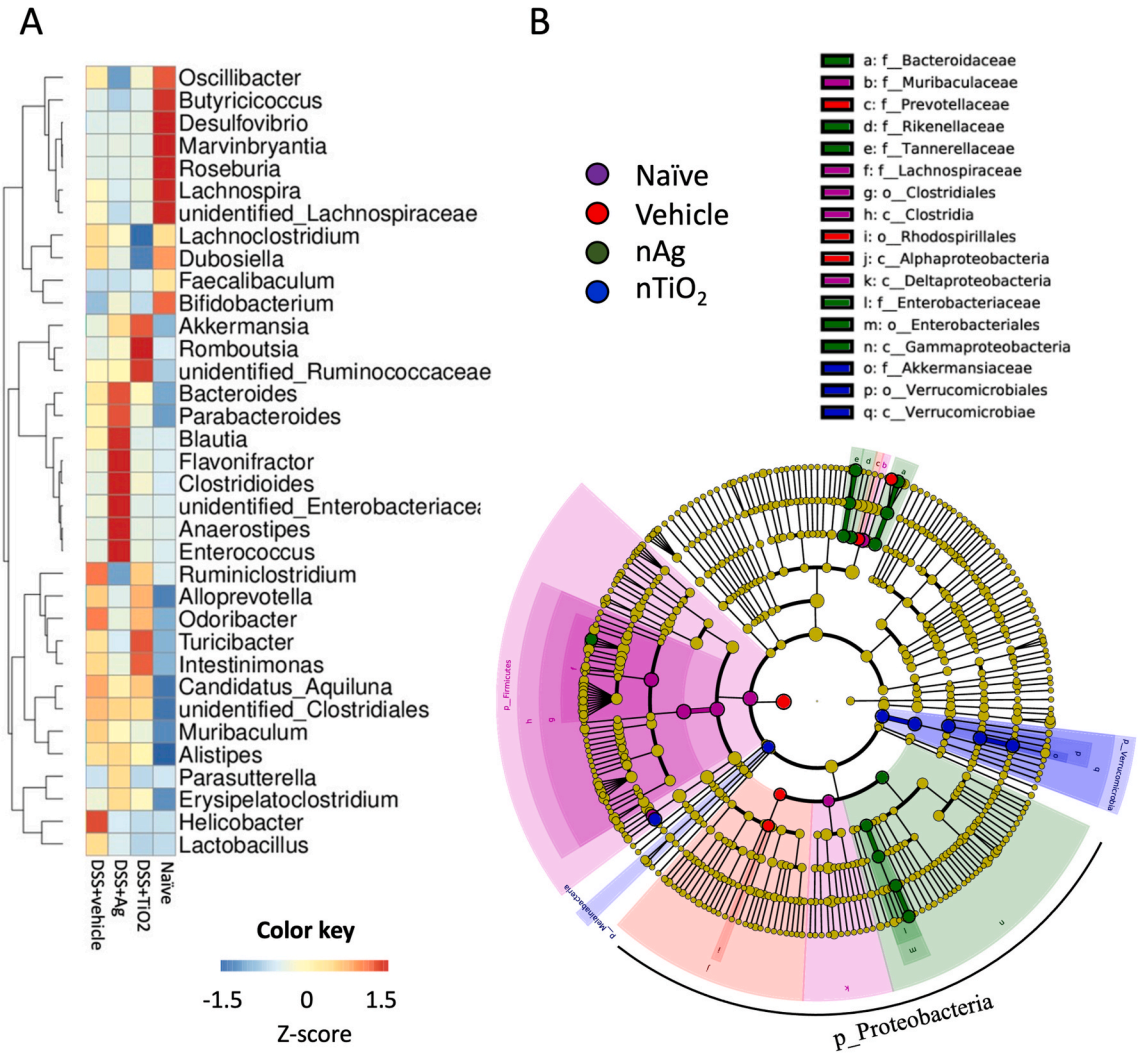

Fig. 5. OTU distribution and clustering of Ag and TiO_2 treated mice. (A) Heatmap of genus-level taxonomic annotation shows the 35 most abundant OTUs among all samples based on relative abundance. The relative values are Z-score normalized and color-coded. Each row represents a genus, and each column represents a treatment group (N = 8/group). Red indicates higher relative abundance. Blue indicates lower relative abundance. (B) Cladograms show the most significant differentially abundant taxa among comparisons with vehicle, Ag and TiO_2 groups in LEfSe analysis. Purple, red, green, and blue colored nodes represent the most differentially abundant bacteria in naïve, vehicle-, nAg-, and $nTiO_2$-treated mice respectively. (For interpretation of the references to color in this figure legend, the reader is referred to the Web version of this article.)

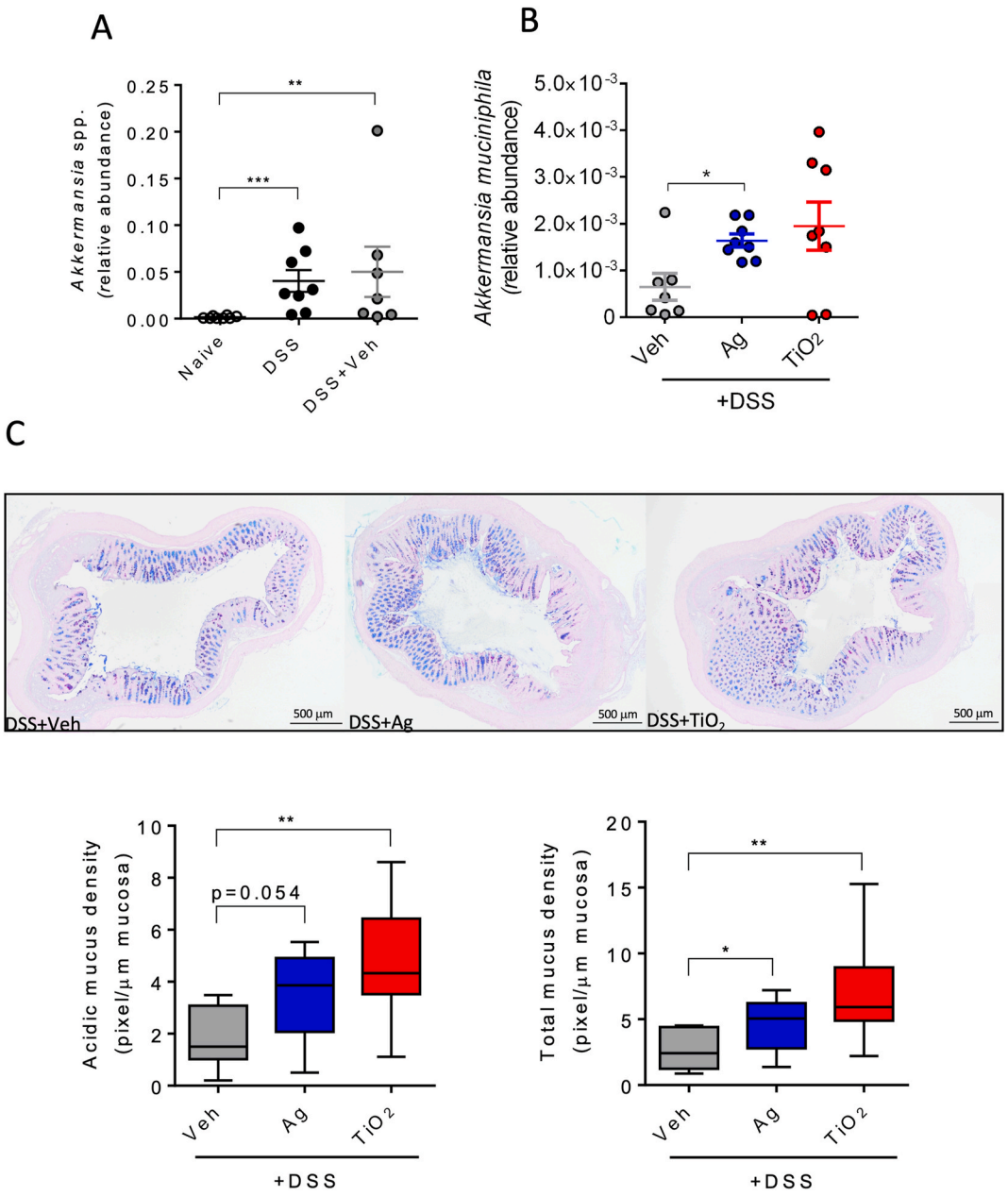

Fig. 6. Relative abundance of *Akkermansia muciniphila* and colonic mucus. (A) Relative abundance of *Akkermansia* spp. in stool of naïve mice, DSS treated mice (DSS) and DSS + Vehicle treated mice (DSS + Veh) is shown. (B) *Akkermansia muciniphilia* is highly present in Ag, and especially, in TiO_2 group. (C) Representative pictures of PAS-AB-stained colon tissue from each group taken at 40x magnification are shown. Blue stain represents acidic mucosubstances while the sum of blue, magenta, and purple stains represents total mucosubstances. The area of acidic and total mucus is shown as stain density via ImageJ. Differences between the groups (N = 8/group) were studied by Mann–Whitney *U* test. Data in A and B represent mean ± SEM, and in C represent min, mean and max, *p < 0.05, **p < 0.01, ***p < 0.001. (For interpretation of the references to color in this figure legend, the reader is referred to the Web version of this article.)

barrier function (Everard et al., 2013). We found that the amount of acidic mucosubstances was increased in colon after nAg and $nTiO_2$ treatment (Fig. 6C). In addition, the total colonic mucosubstances in nanoparticle-fed mice was significantly higher than the vehicle mice, especially after oral exposure to $nTiO_2$ (Fig. 6C).

4. Discussion

The rapid development of nanotechnology has fueled a significant rise in innovations of nanoparticle-based products in the food and household commodity industries, increasing the chance of human oral exposure to them. Characterization of potential toxicities posed by different nanoparticles in individuals under different health conditions is needed to ensure their safety for all consumers. Since the local effect induced by ingested nAg and $nTiO_2$ under an inflammatory condition is not yet completely understood, we sought to investigate the potential toxic or biological effect elicited by these two popular types of metallic nanoparticles in the mouse model of DSS-induced acute colitis. Previous studies have assessed the effect of nAg- or $nTiO_2$-containing food additives, E174 and E171 respectively (Cao et al., 2020; Bettini et al., 2017; EFSA Panel on Food Additives, 2016; Talamini et al., 2019). We did not study these food additives that contain a wide range of particles of different sizes, but instead our aim was to examine the effect of well-characterized model nanoparticles to provide a specific account of their bioactivity *in vivo* and facilitate the comparability to other studies with particles of similar physicochemical properties. We adopted oral

gavage as the ingestion route of nAg or $nTiO_2$ particles in mice. It may not fully mimic oral exposure in real life, and it bypasses the short digestion or incubation of these particles in the oral cavity. Srinivasan et al. revealed distinct protein corona composition profiles upon interaction between saliva protein and nAg or $nTiO_2$ (Srinivasan et al., 2020). Contrarily, an *in vitro* study reported that nAg exhibited great stability in human saliva, with the majority of particles remaining intact and chemically inert after a 24-h incubation (Ngamchuea et al., 2018). Nonetheless, it remains possible that saliva fluid may modify the physicochemical properties (e.g. surface charge, size and dissolution) of these particles and consequently affect their fate along the gastrointestinal tract (Pinďáková et al., 2017; Walczak et al., 2012).

In our colitis model, $nTiO_2$ shortened colon length and deepened infiltration of inflammatory cells, whereas nAg reduced the erosion on the colonic epithelium. Ruiz et al. also showed shortened colon length and worsened histology after 7-day $nTiO_2$ oral gavage in the same acute DSS-colitis model (Ruiz et al., 2017), and Mu et al. showed that $nTiO_2$ aggravated the phenotypes of chronic colitis mice, such as reducing body weight and shortening colon length after three-month exposure to $nTiO_2$ (Mu et al., 2019). NLRP3 inflammasome activation has been suggested as one of the possible mechanisms for the pro-inflammatory effect by $nTiO_2$ (Ruiz et al., 2017). Additionally, gut microbiota dysbiosis induced by $nTiO_2$ has been demonstrated in other studies where alterations at compositional or functional level were associated with development of colonic inflammation (Cao et al., 2020; Mu et al., 2019). The possible mechanisms for $nTiO_2$-induced toxicity involve induction of oxidative stress and DNA damage and activation of inflammatory responses (Gui et al., 2011; Ze et al., 2013; Long et al., 2006). On the other hand, a recent study reported that $nTiO_2$ ameliorated colitis symptoms in a trinitrobenzenesulfonic acid (TNBS)-induced acute colitis model (Gao et al., 2021). TNBS model resembles Crohn's disease, another subtype of IBD, which is mediated by T-cell responses and Th1-type cytokine secretion (Neurath et al., 1995). In contrast, the DSS-colitis model we used mimics ulcerative colitis, where the uncontrolled immune response is mainly driven by innate immunity such as substantial neutrophil infiltration (Chassaing et al., 2014). The differences in pathomechanism of two different disease models may explain the variations in results. However, our studies suggest that ingestion of $nTiO_2$ may worsen existing intestinal inflammation.

After exposure to nAg, we did not see major macroscopic changes in our DSS-colitis model, except for ameliorated epithelial erosion when compared to the vehicle mice. The role of nAg in relation to induction of pro-inflammatory or anti-inflammatory responses is still unclear at this point. Siczek et al. and Krajewska et al. demonstrated that intracolonic administration of nano-scale Ag exerted anti-inflammatory effects and reduced disease severity in DSS-induced colitis in mice (Siczek et al., 2017; Krajewska et al., 2020). Our current results are insufficient to suggest whether nAg could overall ameliorate colitis symptoms. The potential anti-inflammatory effect following the exposure to nAg might be mediated by gut microbiome alterations, such as by increasing number of probiotic *Lactobacillus* spp. (Siczek et al., 2017) Additionally, Yang et al. showed a protective action of nAg on the outcome of rheumatoid arthritis that was associated with induction of M2 macrophage polarization and M1 macrophage apoptosis by the released Ag ions (Yang et al., 2021). On the contrary, Chen et al. demonstrated that oral exposure to nAg induced colitis-like histological damages to the colon of naïve mice (Chen et al., 2017). Multiple potential mechanisms underlying the immunotoxicity induced by nAg has been reported by others, such as through disruption of tight junction proteins(Chen et al., 2017; Williams et al., 2016), generation of oxidative stress (Paino and Zucolotto, 2015; Jia et al., 2020), and activation of transcription factors (Nrf-2 and NF-κB) (Polet et al., 2020; Böhmert et al., 2015). Taken together, more research is still warranted to conclude the nature of the context-dependent potential of immunotoxicological effects posed by nAg, due to the differences in physicochemical properties and doses of nanoparticles used in different experiments, and variations in experimental setups.

In addition to the histological changes, we sought to investigate the local transcriptomic alterations induced by nAg or $nTiO_2$. The PCA analysis and hierarchical clustering of DEGs indicate that nAg, compared to $nTiO_2$, had a greater ability in triggering changes in gene expression pattern of colitis mice. This finding is in line with our previous *in vitro* study using the same particles and showing that nAg, but not $nTiO_2$, could induce significant transcriptional modifications in macrophages (differentiated THP-1 cells) (Poon et al., 2017). In our DSS-colitis model, the nAg-impacted colonic transcriptome was predominantly characterized by downregulated DEGs related to mRNA metabolism and processing. This marked modulation of mRNA molecules and their activities may be an adaptive response to Ag nanoparticles. Dissolved Ag ions could be a source of abiotic stress, leading to suppression of mRNA maturation and the subsequent translation processes. We also found that nAg ingestion may change the regulation of apoptotic cell death. A number of *in vitro* studies in assorted cell lines have demonstrated the induction of apoptosis by nAg (Sanpui et al., 2011; Tang et al., 2019; Kim et al., 2014; Xiao et al., 2019). Various mechanisms of Ag-induced apoptosis have been postulated, such as ROS-induced cellular membrane damage(Quevedo et al., 2021), mitochondrial permeabilization (Su et al., 2019), and increased production of intracellular ROS (Sanpui et al., 2011). In addition, our study shows that lipid catabolism was associated with nAg ingestion in DSS-colitis mice, implying a potential role of nAg in regulation of cellular lipid metabolism.

Gut microbiome has been identified as a key player that has profound impacts on host intestinal and extraintestinal health including IBD(Ni et al., 2017), and several studies have demonstrated that different Ag and TiO_2 nanoparticles are able to alter the gut microbiota profiles in different animal models (Van Den Brûle et al., 2015; Pinget et al., 2019; Wilding et al., 2016; Cho et al., 2013; Li et al., 2018; Mao et al., 2019). In our studies, we saw that $nTiO_2$ decreased the α-diversity and increased Verrucomicrobia, while nAg led to a lowered F/B ratio of gut microbiota likely due to a decreased amount of Firmicutes. A decreased F/B ratio has been suggested to contribute to inflammation in the gut (Stojanov et al., 2020). Our 16S-sequencing data suggest that ingestion of nAg may enhance the pro-inflammatory state in colitis mice. On the contrary, some other studies have shown that nAg increased F/B ratio in healthy mice and rats (Van Den Brûle et al., 2015; Javurek et al., 2017). These findings suggest that nAg given under different contexts may produce different effects on gut microbiota composition.

We observed that some alterations in gut microbiota composition were particle-specific. In our study, nAg-treated mice showed an increased proportion of Proteobacteria phylum, Gammaproteobacteria class in *Enterobacteriaceae* family. Another study also reported that *Enterobacteriaceae* family-specific bacterial gene expression was elevated after consumption of nAg (Williams et al., 2015). An expansion of Proteobacteria has been considered as a pathogenic "microbial signature" that fuels inflammatory disease development (Frank et al., 2007; Shin et al., 2015; Selvanantham et al., 2016; Maharshak et al., 2013; Sartor, 2008; Carvalho et al., 2012). A bloom in *Enterobacteriaceae* family may be a consequence of excess nitrates produced during inflammation that serve as substrates supporting the growth of these bacteria(Winter et al., 2013), thereby being a positive marker of colitis disease severity (de Bruyn et al., 2018; Håkansson et al., 2015). Our data imply that nAg potentiated gut dysbiosis in colitis mice, and it may worsen colon inflammation if such dysbiosis persists. Within the Melainabacteria phylum, *Romboutsia* and *Turicibacter* genera were increased by $nTiO_2$ exposure in our study. Their abundances were also seen enhanced in other colitis or colitis-associated colorectal cancer studies(de Bruyn et al., 2018; Pei et al., 2019; Dou et al., 2020; Wu et al., 2016, 2019; Munyaka et al., 2016), although their biological roles in human health are not yet fully understood. Given the shortened colon and deeper inflammation induced by $nTiO_2$ in our study, increases in *Romboutsia* and *Turicibacter* species may be potential indicators of enhanced

inflammation in the gut.

We found that both nAg and $nTiO_2$ particles enhanced the amount of total and acidic mucosubstances in the colon. Jeong et al. and Dorier et al. reported that oral administration of nAg and $nTiO_2$ promoted the mucus secretion in the gut of healthy rats and Caco-2/HT29-MTX intestinal cells respectively (Jeong et al., 2010; Dorier et al., 2019). Mucus layer in the colon forms a critical physical barrier for host defense against food-associated and microbial antigens. Our data show that nAg and $nTiO_2$ are potential stimuli that enhance intestinal mucus production. Furthermore, we noted that the increased level of mucus was positively correlated with an increased proportion of *Akkermansia muciniphila*, one of the most studied mucus-inhabiting genus that attaches to mucus and uses it as an energy source when food-derived carbohydrates are in short supply (Johansson et al., 2011; Hansson, 2020). We observed that DSS treatment led to an enhanced load of *Akkermansia* spp. in stool when compared to the naïve mice, suggesting a positive association between *Akkermansia* spp. and development of colitis. In addition, we showed that nAg and $nTiO_2$ exposure in addition to DSS further produced an increase in *Akkermansia muciniphila*. Similarly, a significant enrichment of *Akkermansia muciniphila* has been documented in acute DSS models and patients with colorectal cancer and cholecystitis in other studies (Håkansson et al., 2015; Sasso et al., 2020; Zhang et al., 2016; Borton et al., 2017; Weir et al., 2013; Liu et al., 2015). We suggest that *Akkermansia muciniphila* bloom may be an adaptive response to colon inflammation or promote the development of colitis.

In this study, we chose a disease model to examine the modulating effect caused by nAg and $nTiO_2$ in gut microbiota under an inflammatory condition, which sought to examine the potential nanoparticle-induced harms in people suffering from IBD. Nonetheless, data on nanoparticles-induced microbial changes in healthy mice are still needed to reveal their impact on the healthy population. Although the doses used in this study can reflect the higher intake of nAg and $nTiO_2$ from people having a biased diet (e.g. habitual eaters of candies or coffer creamers), they may be an over-estimation when individuals follow the health recommendations of eating diverse food types. The selection of test doses for nanoparticle toxicity evaluation is often a compromise since the actual and most updated exposure levels are not fully known. Nonetheless, different doses are needed to facilitate interpretation of assay results for the heterogenous population. Future studies with multiple doses, longer and chronic exposure period, and several time points need to be considered to investigate the long-term toxicities and other influences caused by these nanoparticles at varied doses on the gut microbiota and gut immunity.

To conclude, we reported here the biological effect of oral exposure to nAg or $nTiO_2$ in the context of DSS-induced colitis in mice, supported by data generated from RNA sequencing and 16S sequencing. We found that nAg and $nTiO_2$ induce dissimilar immunotoxicological changes at the molecular and microbiome level. Our results show that nAg and $nTiO_2$ caused varied degrees of gut transcriptomic and microbiome alterations under an inflammatory condition. NAg significantly affected mRNA metabolism/processing and apoptosis in the colon. It also induced gut dysbiosis that might promote inflammation. $NTiO_2$ induced mild transcriptional changes. The local damaging effect caused by $nTiO_2$ might be associated with increases in *Romboutsia* and *Turicibacter* species. Notably, both particles stimulated the production of mucus in the colon and the growth of potentially pro-inflammatory *Akkermansia muciniphila*. Our findings provide evidence for regulatory authorities, policy makers, and the general public to keep in mind the cautionary use of nAg- and $nTiO_2$-containing food products.

Funding

The study was supported by a grant from the Academy of Finland (decision 307768).

Availability of data and materials

The datasets used and/or analyzed during the current study are available from the corresponding author on reasonable request.

Ethics approval and consent to participate

All experimental mice were provided with humane care. The study was conducted in accordance with the guidelines and regulations of University of Hong Kong and the Department of Health of the HKSAR Government for animal experiments, and received approval from the Committee on the Use of Live Animals in Teaching and Research (CULATR) of the University of Hong Kong (Approval number: 5228-19) and the Department of Health of the Hong Kong Special Administrative Region (HKSAR) Government (License number: 19–1200 in DH/SHS/8/2/3 Pt.40).

Consent for publication

Not applicable.

CRediT authorship contribution statement

Shuyuan Wang: Study design, Animal experimentation, Sample preparation, Formal analysis, (including statistics) of experimental parameters, Visualization, Writing – original draft, Writing – review & editing. **Xing Kang:** Formal analysis, (including statistics) of experimental parameters. **Harri Alenius:** Writing – review & editing. **Sunny Hei Wong:** Writing – review & editing. **Piia Karisola:** Study design, Bioinformatic, Formal analysis, Analysis (including statistics) of experimental parameters, Visualization, Supervision, Writing – review & editing, Project administration. **Hani El-Nezami:** Study design, Supervision, Writing – review & editing, Project administration.

Declaration of competing interest

The authors declare that they have no known competing financial interests or personal relationships that could have appeared to influence the work reported in this paper.

Data availability

Data will be made available on request.

Acknowledgements

We thank the RNA sequencing service provided by the Biomedicum Functional Genomics Unit (FUGU) at the Helsinki Institute of Life Science and Biocenter Finland at the University of Helsinki, and the 16S sequencing service conducted by Novogenes Co., Ltd.

Abbreviations

Ag	Silver
DAI	Disease activity index
DSS	Dextran sulphate sodium
GO	Gene Ontology
IBD	Inflammatory bowel disease
IPA	Ingenuity Pathway Analysis
LDA	Linear discriminant analysis
LefSe	Linear discriminant analysis effect size
MAPK	Mitogen-activated protein kinase
PAS-AB	Periodic acid schiff-alcian blue
PCA	Principal component analysis
PVP	Polyvinylpyrrolidone
ROS	Reactive oxidative species

TiO_2	Titanium dioxide
TMM	Trimmed Mean of M-values
UC	Ulcerative colitis

Appendix A. Supplementary data

Supplementary data to this article can be found online at https://doi.org/10.1016/j.fct.2022.113368.

References

Amat, C.B., Motta, J.-P., Fekete, E., Moreau, F., Chadee, K., Buret, A.G., 2017. Cysteine protease–dependent mucous disruptions and differential mucin gene expression in Giardia duodenalis infection. Am. J. Pathol. 187 (11), 2486–2498.

Baumgart, M., Dogan, B., Rishniw, M., Weitzman, G., Bosworth, B., Yantiss, R., et al., 2007. Culture independent analysis of ileal mucosa reveals a selective increase in invasive Escherichia coli of novel phylogeny relative to depletion of Clostridiales in Crohn's disease involving the ileum. ISME J. 1 (5), 403–418.

Bettini, S., Boutet-Robinet, E., Cartier, C., Coméra, C., Gaultier, E., Dupuy, J., et al., 2017. Food-grade TiO 2 impairs intestinal and systemic immune homeostasis, initiates preneoplastic lesions and promotes aberrant crypt development in the rat colon. Sci. Rep. 7 (1), 1–13.

Böhmert, L., Niemann, B., Lichtenstein, D., Juling, S., Lampen, A., 2015. Molecular mechanism of silver nanoparticles in human intestinal cells. Nanotoxicology 9 (7), 852–860.

Bokulich, N.A., Subramanian, S., Faith, J.J., Gevers, D., Gordon, J.I., Knight, R., et al., 2013. Quality-filtering vastly improves diversity estimates from Illumina amplicon sequencing. Nat. Methods 10 (1), 57–59.

Borton, M.A., Sabag-Daigle, A., Wu, J., Solden, L.M., O'Banion, B.S., Daly, R.A., et al., 2017. Chemical and pathogen-induced inflammation disrupt the murine intestinal microbiome. Microbiome 5 (1), 1–15.

Cao, X., Han, Y., Gu, M., Du, H., Song, M., Zhu, X., et al., 2020. Foodborne titanium dioxide nanoparticles induce stronger adverse effects in obese mice than non-obese mice: gut microbiota dysbiosis, colonic inflammation, and proteome alterations. Small 16 (36) e2001858-n/a.

Caporaso, J.G., Kuczynski, J., Stombaugh, J., Bittinger, K., Bushman, F.D., Costello, E.K., et al., 2010. QIIME allows analysis of high-throughput community sequencing data. Nat. Methods 7 (5), 335–336.

Carvalho, F.A., Koren, O., Goodrich, J.K., Johansson, M.E., Nalbantoglu, I., Aitken, J.D., et al., 2012. Transient inability to manage proteobacteria promotes chronic gut inflammation in TLR5-deficient mice. Cell Host Microbe 12 (2), 139–152.

Chassaing, B., Aitken, J.D., Malleshappa, M., Vijay-Kumar, M., 2014. Dextran sulfate sodium (DSS)-induced colitis in mice. Curr. Protoc. Im. 104 (1), 15.25. 11-15.25. 14.

Chaudhry, Q., Scotter, M., Blackburn, J., Ross, B., Boxall, A., Castle, L., et al., 2008. Applications and implications of nanotechnologies for the food sector. Food Addit. Contam. 25 (3), 241–258.

Chen, H., Zhao, R., Wang, B., Cai, C., Zheng, L., Wang, H., et al., 2017. The effects of orally administered Ag, TiO2 and SiO2 nanoparticles on gut microbiota composition and colitis induction in mice. NanoImpact 8, 80–88.

Cho, W.-S., Kang, B.-C., Lee, J.K., Jeong, J., Che, J.-H., Seok, S.H., 2013. Comparative absorption, distribution, and excretion of titanium dioxide and zinc oxide nanoparticles after repeated oral administration. Part. Fibre Toxicol. 10 (1), 1–9.

de Bruyn, M., Sabino, J., Vandeputte, D., Vermeire, S., Raes, J., Opdenakker, G., 2018. Comparisons of gut microbiota profiles in wild-type and gelatinase B/matrix metalloproteinase-9-deficient mice in acute DSS-induced colitis. NPJ biofilms and microbiomes 4 (1), 1–9.

Dorier, M., Béal, D., Tisseyre, C., Marie-Desvergne, C., Dubosson, M., Barreau, F., et al., 2019. The food additive E171 and titanium dioxide nanoparticles indirectly alter the homeostasis of human intestinal epithelial cells in vitro. Environ. Sci. .: Nano 6 (5), 1549–1561.

Dou, X., Gao, N., Yan, D., Shan, A., 2020. Sodium butyrate alleviates mouse colitis by regulating gut microbiota dysbiosis. Animals 10 (7), 1154.

Duboc, H., Rajca, S., Rainteau, D., Benarous, D., Maubert, M.-A., Quervain, E., et al., 2013. Connecting dysbiosis, bile-acid dysmetabolism and gut inflammation in inflammatory bowel diseases. Gut 62 (4), 531–539.

Edelblum, K.L., Turner, J.R., 2009. The tight junction in inflammatory disease: communication breakdown. Curr. Opin. Pharmacol. 9 (6), 715–720.

Edgar, R.C., 2013. UPARSE: highly accurate OTU sequences from microbial amplicon reads. Nat. Methods 10 (10), 996–998.

Edgar, R.C., Haas, B.J., Clemente, J.C., Quince, C., Knight, R., 2011. UCHIME improves sensitivity and speed of chimera detection. Bioinformatics 27 (16), 2194–2200.

EFSA Panel on Food Additives Nutrient Sources added to Food. Scientific opinion on the re-evaluation of silver (E 174) as food additive. EFSA J. 14 (1), 2016, 4364.

Erben, U., Loddenkemper, C., Doerfel, K., Spieckermann, S., Haller, D., Heimesaat, M.M., et al., 2014. A guide to histomorphological evaluation of intestinal inflammation in mouse models. Int. J. Clin. Exp. Pathol. 7 (8), 4557.

European Commission, 2021. Re-evaluation [cited 2021 Nov 9, 2021]; Available from: https://ec.europa.eu/food/safety/food-improvement-agents/additives/re-evaluation_en#ecl-inpage-779.

Everard, A., Belzer, C., Geurts, L., Ouwerkerk, J.P., Druart, C., Bindels, L.B., et al., 2013. Cross-talk between Akkermansia muciniphila and intestinal epithelium controls diet-induced obesity. Proc. Natl. Acad. Sci. USA 110 (22), 9066–9071.

Frank, D.N., Amand, A.L.S., Feldman, R.A., Boedeker, E.C., Harpaz, N., Pace, N.R., 2007. Molecular-phylogenetic characterization of microbial community imbalances in human inflammatory bowel diseases. Proc. Natl. Acad. Sci. USA 104 (34), 13780–13785.

Gao, Y., Li, T., Duan, S., Lyu, L., Li, Y., Xu, L., et al., 2021. Impact of titanium dioxide nanoparticles on intestinal community in 2, 4, 6-trinitrobenzenesulfonic acid (TNBS)-induced acute colitis mice and the intervention effect of vitamin E. Nanoscale 13 (3), 1842–1862.

Gui, S., Zhang, Z., Zheng, L., Cui, Y., Liu, X., Li, N., et al., 2011. Molecular mechanism of kidney injury of mice caused by exposure to titanium dioxide nanoparticles. J. Hazard Mater. 195, 365–370.

Håkansson, Å., Tormo-Badia, N., Baridi, A., Xu, J., Molin, G., Hagslätt, M.-L., et al., 2015. Immunological alteration and changes of gut microbiota after dextran sulfate sodium (DSS) administration in mice. Clin. Exp. Med. 15 (1), 107–120.

Halfvarson, J., Brislawn, C.J., Lamendella, R., Vázquez-Baeza, Y., Walters, W.A., Bramer, L.M., et al., 2017. Dynamics of the human gut microbiome in inflammatory bowel disease. Nature microbiology 2 (5), 1–7.

Hansson, G.C., 2020. Mucins and the microbiome. Annu. Rev. Biochem. 89, 769–793.

Javurek, A.B., Suresh, D., Spollen, W.G., Hart, M.L., Hansen, S.A., Ellersieck, M.R., et al., 2017. Gut dysbiosis and neurobehavioral alterations in rats exposed to silver nanoparticles. Sci. Rep. 7 (1), 1–15.

Jeong, G.N., Jo, U.B., Ryu, H.Y., Kim, Y.S., Song, K.S., Yu, I.J., 2010. Histochemical study of intestinal mucins after administration of silver nanoparticles in Sprague–Dawley rats. Arch. Toxicol. 84 (1), 63–69.

Jia, M., Zhang, W., He, T., Shu, M., Deng, J., Wang, J., et al., 2020. Evaluation of the genotoxic and oxidative damage potential of silver nanoparticles in human NCM460 and HCT116 cells. Int. J. Mol. Sci. 21 (5), 1618.

Johansson, M.E., Ambort, D., Pelaseyed, T., Schütte, A., Gustafsson, J.K., Ermund, A., et al., 2011. Composition and functional role of the mucus layers in the intestine. Cell. Mol. Life Sci. 68 (22), 3635–3641.

Kim, S.-H., Ko, J.-W., Koh, S.-K., Lee, I.-C., Son, J.-M., Moon, C., et al., 2014. Silver nanoparticles induce apoptotic cell death in cultured cerebral cortical neurons. Molecular & Cellular Toxicology 10 (2), 173–179.

Krajewska, J.B., Długosz, O., Sałaga, M., Banach, M., Fichna, J., 2020. Silver nanoparticles based on blackcurrant extract show potent anti-inflammatory effect in vitro and in DSS-induced colitis in mice. Int. J. Pharm. 585, 119549.

Krämer, A., Green, J., Pollard Jr., J., Tugendreich, S., 2014. Causal analysis approaches in ingenuity pathway analysis. Bioinformatics 30 (4), 523–530.

Langille, M.G., Meehan, C.J., Koenig, J.E., Dhanani, A.S., Rose, R.A., Howlett, S.E., et al., 2014. Microbial shifts in the aging mouse gut. Microbiome 2 (1), 1–12.

Li, J., Yang, S., Lei, R., Gu, W., Qin, Y., Ma, S., et al., 2018. Oral administration of rutile and anatase TiO 2 nanoparticles shifts mouse gut microbiota structure. Nanoscale 10 (16), 7736–7745.

Liu, J., Yan, Q., Luo, F., Shang, D., Wu, D., Zhang, H., et al., 2015. Acute cholecystitis associated with infection of Enterobacteriaceae from gut microbiota. Clin. Microbiol. Infect. 21 (9), 851. e851-851. e859.

Livraghi, A., Grubb, B.R., Hudson, E.J., Wilkinson, K.J., Sheehan, J.K., Mall, M.A., et al., 2009. Airway and lung pathology due to mucosal surface dehydration in β-epithelial Na+ channel-overexpressing mice: role of TNF-α and IL-4Rα signaling, influence of neonatal development, and limited efficacy of glucocorticoid treatment. J. Immunol. 182 (7), 4357–4367.

Lomer, M.C., Thompson, R.P., Powell, J.J., 2002. Fine and ultrafine particles of the diet: influence on the mucosal immune response and association with Crohn's disease. Proc. Nutr. Soc. 61 (1), 123–130.

Lomer, M.C., Hutchinson, C., Volkert, S., Greenfield, S.M., Catterall, A., Thompson, R.P., et al., 2004. Dietary sources of inorganic microparticles and their intake in healthy subjects and patients with Crohn's disease. Br. J. Nutr. 92 (6), 947–955.

Long, T.C., Saleh, N., Tilton, R.D., Lowry, G.V., Veronesi, B., 2006. Titanium dioxide (P25) produces reactive oxygen species in immortalized brain microglia (BV2): implications for nanoparticle neurotoxicity. Environ. Sci. Technol. 40 (14), 4346–4352.

Macosko, E.Z., Basu, A., Satija, R., Nemesh, J., Shekhar, K., Goldman, M., et al., 2015. Highly parallel genome-wide expression profiling of individual cells using nanoliter droplets. Cell 161 (5), 1202–1214.

Magoč, T., Salzberg, S.L., 2011. FLASH: fast length adjustment of short reads to improve genome assemblies. Bioinformatics 27 (21), 2957–2963.

Maharshak, N., Packey, C.D., Ellermann, M., Manick, S., Siddle, J.P., Huh, E.Y., et al., 2013. Altered enteric microbiota ecology in interleukin 10-deficient mice during development and progression of intestinal inflammation. Gut Microb. 4 (4), 316–324.

Maloy, K.J., Powrie, F., 2011. Intestinal homeostasis and its breakdown in inflammatory bowel disease. Nature 474 (7351), 298–306.

Manichanh, C., Rigottier-Gois, L., Bonnaud, E., Gloux, K., Pelletier, E., Frangeul, L., et al., 2006. Reduced diversity of faecal microbiota in Crohn's disease revealed by a metagenomic approach. Gut 55 (2), 205–211.

Mao, Z., Li, Y., Dong, T., Zhang, L., Zhang, Y., Li, S., et al., 2019. Exposure to titanium dioxide nanoparticles during pregnancy changed maternal gut microbiota and increased blood glucose of rat. Nanoscale Res. Lett. 14 (1), 1–8.

Medina-Reyes, E.I., Rodríguez-Ibarra, C., Déciga-Alcaraz, A., Díaz-Urbina, D., Chirino, Y. I., Pedraza-Chaverri, J., 2020. Food additives containing nanoparticles induce gastrotoxicity, hepatotoxicity and alterations in animal behavior: the unknown role of oxidative stress. Food Chem. Toxicol., 111814

Mi, H., Huang, X., Muruganujan, A., Tang, H., Mills, C., Kang, D., et al., 2017. PANTHER version 11: expanded annotation data from Gene Ontology and Reactome pathways, and data analysis tool enhancements. Nucleic Acids Res. 45 (D1), D183–D189.

Mu, W., Wang, Y., Huang, C., Fu, Y., Li, J., Wang, H., et al., 2019. Effect of long-term intake of dietary titanium dioxide nanoparticles on intestine inflammation in mice. J. Agric. Food Chem. 67 (33), 9382–9389.
Munyaka, P.M., Rabbi, M.F., Khafipour, E., Ghia, J.E., 2016. Acute dextran sulfate sodium (DSS)-induced colitis promotes gut microbial dysbiosis in mice. J. Basic Microbiol. 56 (9), 986–998.
Murano, M., Maemura, K., Hirata, I., Toshina, K., Nishikawa, T., Hamamoto, N., et al., 2000. Therapeutic effect of intracolonically administered nuclear factor κB (p65) antisense oligonucleotide on mouse dextran sulphate sodium (DSS)-induced colitis. Clin. Exp. Immunol. 120 (1), 51–58.
Nagao-Kitamoto, H., Shreiner, A.B., Gillilland III, M.G., Kitamoto, S., Ishii, C., Hirayama, A., et al., 2016. Functional characterization of inflammatory bowel disease–associated gut dysbiosis in gnotobiotic mice. Cellular and molecular gastroenterology and hepatology 2 (4), 468–481.
Neurath, M.F., Fuss, I., Kelsall, B.L., Stüber, E., Strober, W., 1995. Antibodies to interleukin 12 abrogate established experimental colitis in mice. J. Exp. Med. 182 (5), 1281–1290.
Ngamchuea, K., Batchelor-McAuley, C., Compton, R.G., 2018. The fate of silver nanoparticles in authentic human saliva. Nanotoxicology 12 (4), 305–311.
Ni, J., Wu, G.D., Albenberg, L., Tomov, V.T., 2017. Gut microbiota and IBD: causation or correlation? Nat. Rev. Gastroenterol. Hepatol. 14 (10), 573–584.
Oliveros, Venny, J.C.. An interactive tool for comparing lists with Venn's diagrams. 2007-2015 [cited 2021 5 July]; Available from: https://bioinfogp.cnb.csic.es/tools/venny/index.html.
Paino, I.M.M., Zucolotto, V., 2015. Poly (vinyl alcohol)-coated silver nanoparticles: activation of neutrophils and nanotoxicology effects in human hepatocarcinoma and mononuclear cells. Environ. Toxicol. Pharmacol. 39 (2), 614–621.
Panpetch, W., Hiengrach, P., Nilgate, S., Tumwasorn, S., Somboonna, N., Wilantho, A., et al., 2020. Additional Candida albicans administration enhances the severity of dextran sulfate solution induced colitis mouse model through leaky gut-enhanced systemic inflammation and gut-dysbiosis but attenuated by Lactobacillus rhamnosus L34. Gut Microb. 11 (3), 465–480.
Park, E.-J., Bae, E., Yi, J., Kim, Y., Choi, K., Lee, S.H., et al., 2010. Repeated-dose toxicity and inflammatory responses in mice by oral administration of silver nanoparticles. Environ. Toxicol. Pharmacol. 30 (2), 162–168.
Pei, L-y, Ke, Y-s, Zhao, H-h, Wang, L., Jia, C., Liu, W-z, et al., 2019. Role of colonic microbiota in the pathogenesis of ulcerative colitis. BMC Gastroenterol. 19 (1), 1–11.
Peters, R.J., van Bemmel, G., Herrera-Rivera, Z., Helsper, H.P., Marvin, H.J., Weigel, S., et al., 2014. Characterization of titanium dioxide nanoparticles in food products: analytical methods to define nanoparticles. J. Agric. Food Chem. 62 (27), 6285–6293.
Pinďáková, L., Kašpárková, V., Kejlová, K., Dvořáková, M., Krsek, D., Jírová, D., et al., 2017. Behaviour of silver nanoparticles in simulated saliva and gastrointestinal fluids. Int. J. Pharm. 527 (1–2), 12–20.
Pinget, G., Tan, J., Janac, B., Kaakoush, N.O., Angelatos, A.S., O'Sullivan, J., et al., 2019. Impact of the food additive titanium dioxide (E171) on gut microbiota-host interaction. Front. Nutr. 6, 57.
Polet, M., Laloux, L., Cambier, S., Ziebel, J., Gutleb, A.C., Schneider, Y.-J., 2020. Soluble silver ions from silver nanoparticles induce a polarised secretion of interleukin-8 in differentiated Caco-2 cells. Toxicol. Lett. 325, 14–24.
Poon, W.-L., Alenius, H., Ndika, J., Fortino, V., Kolhinen, V., Meščeriakovas, A., et al., 2017. Nano-sized zinc oxide and silver, but not titanium dioxide, induce innate and adaptive immunity and antiviral response in differentiated THP-1 cells. Nanotoxicology 11 (7), 936–951.
Quast, C., Pruesse, E., Yilmaz, P., Gerken, J., Schweer, T., Yarza, P., et al., 2012. The SILVA ribosomal RNA gene database project: improved data processing and web-based tools. Nucleic Acids Res. 41 (D1), D590–D596.
Quevedo, A.C., Lynch, I., Valsami-Jones, E., 2021. Silver nanoparticle induced toxicity and cell death mechanisms in embryonic zebrafish cells. Nanoscale 13 (12), 6142–6161.
Rajca, S., Grondin, V., Louis, E., Vernier-Massouille, G., Grimaud, J.-C., Bouhnik, Y., et al., 2014. Alterations in the intestinal microbiome (dysbiosis) as a predictor of relapse after infliximab withdrawal in Crohn's disease. Inflamm. Bowel Dis. 20 (6), 978–986.
Ruiz, P.A., Morón, B., Becker, H.M., Lang, S., Atrott, K., Spalinger, M.R., et al., 2017. Titanium dioxide nanoparticles exacerbate DSS-induced colitis: role of the NLRP3 inflammasome. Gut 66 (7), 1216–1224.
Sanpui, P., Chattopadhyay, A., Ghosh, S.S., 2011. Induction of apoptosis in cancer cells at low silver nanoparticle concentrations using chitosan nanocarrier. ACS Appl. Mater. Interfaces 3 (2), 218–228.
Sartor, R.B., 2008. Microbial influences in inflammatory bowel diseases. Gastroenterology 134 (2), 577–594.
Sasso, G.L., Phillips, B.W., Sewer, A., Battey, J.N., Kondylis, A., Talikka, M., et al., 2020. The reduction of DSS-induced colitis severity in mice exposed to cigarette smoke is linked to immune modulation and microbial shifts. Sci. Rep. 10 (1), 1–18.
Seekatz, A.M., Aas, J., Gessert, C.E., Rubin, T.A., Saman, D.M., Bakken, J.S., et al., 2014. Recovery of the gut microbiome following fecal microbiota transplantation. mBio 5 (3) e00893-00814.
Seksik, P., Rigottier-Gois, L., Gramet, G., Sutren, M., Pochart, P., Marteau, P., et al., 2003. Alterations of the dominant faecal bacterial groups in patients with Crohn's disease of the colon. Gut 52 (2), 237–242.
Selvanantham, T., Lin, Q., Guo, C.X., Surendra, A., Fieve, S., Escalante, N.K., et al., 2016. NKT cell–deficient mice harbor an altered microbiota that fuels intestinal inflammation during chemically induced colitis. J. Immunol. 197 (11), 4464–4472.
Shahare, B., Yashpal, M., Gajendra, 2013. Toxic effects of repeated oral exposure of silver nanoparticles on small intestine mucosa of mice. Toxicol. Mech. Methods 23 (3), 161–167.
Shin, N.-R., Whon, T.W., Bae, J.-W., 2015. Proteobacteria: microbial signature of dysbiosis in gut microbiota. Trends Biotechnol. 33 (9), 496–503.
Siczek, K., Zatorski, H., Chmielowiec-Korzeniowska, A., Pulit-Prociak, J., Śmiech, M., Kordek, R., et al., 2017. Synthesis and evaluation of anti-inflammatory properties of silver nanoparticle suspensions in experimental colitis in mice. Chem. Biol. Drug Des. 89 (4), 538–547.
Söderholm, J.D., Olaison, G., Peterson, K., Franzen, L., Lindmark, T., Wirén, M., et al., 2002. Augmented increase in tight junction permeability by luminal stimuli in the non-inflamed ileum of Crohn's disease. Gut 50 (3), 307–313.
Srinivas, P.R., Philbert, M., Vu, T.Q., Huang, Q., Kokini, J.L., Saos, E., et al., 2010. Nanotechnology research: applications in nutritional sciences. J. Nutr. 140 (1), 119–124.
Srinivasan, D., Phue, W.H., Xu, K., George, S., 2020. The type of dietary nanoparticles influences salivary protein corona composition. NanoImpact 19, 100238.
Stojanov, S., Berlec, A., Štrukelj, B., 2020. The influence of probiotics on the Firmicutes/Bacteroidetes ratio in the treatment of obesity and inflammatory bowel disease. Microorganisms 8 (11), 1715.
Su, L.-J., Zhang, J.-H., Gomez, H., Murugan, R., Hong, X., Xu, D., et al., 2019. Reactive oxygen species-induced lipid peroxidation in apoptosis, autophagy, and ferroptosis. Oxid. Med. Cell. Longev 2019, 5080843. https://doi.org/10.1155/2019/5080843.
Talamini, L., Gimondi, S., Violatto, M.B., Fiordaliso, F., Pedica, F., Tran, N.L., et al., 2019. Repeated administration of the food additive E171 to mice results in accumulation in intestine and liver and promotes an inflammatory status. Nanotoxicology 13 (8), 1087–1101.
Tang, J., Lu, X., Chen, B., Cai, E., Liu, W., Jiang, J., et al., 2019. Mechanisms of silver nanoparticles-induced cytotoxicity and apoptosis in rat tracheal epithelial cells. J. Toxicol. Sci. 44 (3), 155–165.
Tyanova, S., Temu, T., Sinitcyn, P., Carlson, A., Hein, M.Y., Geiger, T., et al., 2016. The Perseus computational platform for comprehensive analysis of (prote) omics data. Nat. Methods 13 (9), 731–740.
United States Food and Drug Administration, 2017. Summary of color additives for use in the United States in foods, drugs, cosmetics, and medical devices [cited; Available from: https://www.fda.gov/industry/color-additive-inventories/summarycolor-additives-use-united-states-foods-drugs-cosmetics-and-medical-devices.
Van Den Brûle, S., Ambroise, J., Lecloux, H., Levard, C., Soulas, R., De Temmerman, P.-J., et al., 2015. Dietary silver nanoparticles can disturb the gut microbiota in mice. Part. Fibre Toxicol. 13 (1), 1–16.
van der Zande, M., Vandebriel, R.J., Van Doren, E., Kramer, E., Herrera Rivera, Z., Serrano-Rojero, C.S., et al., 2012. Distribution, elimination, and toxicity of silver nanoparticles and silver ions in rats after 28-day oral exposure. ACS Nano 6 (8), 7427–7442.
Waegeneers, N., De Vos, S., Verleysen, E., Ruttens, A., Mast, J., 2019. Estimation of the uncertainties related to the measurement of the size and quantities of individual silver nanoparticles in confectionery. Materials 12 (17), 2677.
Walczak, A.P., Fokkink, R., Peters, R., Tromp, P., Herrera Rivera, Z.E., Rietjens, I.M., et al., 2012. Behaviour of silver nanoparticles and silver ions in an in vitro human gastrointestinal digestion model. Nanotoxicology 7 (7), 1198–1210.
Walker, A.W., Sanderson, J.D., Churcher, C., Parkes, G.C., Hudspith, B.N., Rayment, N., et al., 2011. High-throughput clone library analysis of the mucosa-associated microbiota reveals dysbiosis and differences between inflamed and non-inflamed regions of the intestine in inflammatory bowel disease. BMC Microbiol. 11 (1), 1–12.
Wang, J., Zhou, G., Chen, C., Yu, H., Wang, T., Ma, Y., et al., 2007a. Acute toxicity and biodistribution of different sized titanium dioxide particles in mice after oral administration. Toxicol. Lett. 168 (2), 176–185.
Wang, Q., Garrity, G.M., Tiedje, J.M., Cole, J.R., 2007b. Naive Bayesian classifier for rapid assignment of rRNA sequences into the new bacterial taxonomy. Appl. Environ. Microbiol. 73 (16), 5261–5267.
Wang, Y., Chen, Z., Ba, T., Pu, J., Chen, T., Song, Y., et al., 2013. Susceptibility of young and adult rats to the oral toxicity of titanium dioxide nanoparticles. Small 9 (9-10), 1742–1752.
Weir, A., Westerhoff, P., Fabricius, L., Hristovski, K., Von Goetz, N., 2012. Titanium dioxide nanoparticles in food and personal care products. Environ. Sci. Technol. 46 (4), 2242–2250.
Weir, T.L., Manter, D.K., Sheflin, A.M., Barnett, B.A., Heuberger, A.L., Ryan, E.P., 2013. Stool microbiome and metabolome differences between colorectal cancer patients and healthy adults. PLoS One 8 (8), e70803.
Wilding, L.A., Bassis, C.M., Walacavage, K., Hashway, S., Leroueil, P.R., Morishita, M., et al., 2016. Repeated dose (28-day) administration of silver nanoparticles of varied size and coating does not significantly alter the indigenous murine gut microbiome. Nanotoxicology 10 (5), 513–520.
Williams, K., Milner, J., Boudreau, M.D., Gokulan, K., Cerniglia, C.E., Khare, S., 2015. Effects of subchronic exposure of silver nanoparticles on intestinal microbiota and gut-associated immune responses in the ileum of Sprague-Dawley rats. Nanotoxicology 9 (3), 279–289.
Williams, K.M., Gokulan, K., Cerniglia, C.E., Khare, S., 2016. Size and dose dependent effects of silver nanoparticle exposure on intestinal permeability in an in vitro model of the human gut epithelium. J. Nanobiotechnol. 14 (1), 1–13.
Winter, S.E., Winter, M.G., Xavier, M.N., Thiennimitr, P., Poon, V., Keestra, A.M., et al., 2013. Host-derived nitrate boosts growth of E. coli in the inflamed gut. Science 339 (6120), 708–711.
Wu, M., Wu, Y., Deng, B., Li, J., Cao, H., Qu, Y., et al., 2016. Isoliquiritigenin decreases the incidence of colitis-associated colorectal cancer by modulating the intestinal microbiota. Oncotarget 7 (51), 85318.

Wu, M., Li, J., An, Y., Li, P., Xiong, W., Li, J., et al., 2019. Chitooligosaccharides prevents the development of colitis-associated colorectal cancer by modulating the intestinal microbiota and mycobiota. Front. Microbiol. 10, 2101.

Xiao, H., Chen, Y., Alnaggar, M., 2019. Silver nanoparticles induce cell death of colon cancer cells through impairing cytoskeleton and membrane nanostructure. Micron 126, 102750.

Yang, Y., Guo, L., Wang, Z., Liu, P., Liu, X., Ding, J., et al., 2021. Targeted silver nanoparticles for rheumatoid arthritis therapy via macrophage apoptosis and Re-polarization. Biomaterials 264, 120390.

Ze, Y., Zheng, L., Zhao, X., Gui, S., Sang, X., Su, J., et al., 2013. Molecular mechanism of titanium dioxide nanoparticles-induced oxidative injury in the brain of mice. Chemosphere 92 (9), 1183–1189.

Zhang, Q., Wu, Y., Wang, J., Wu, G., Long, W., Xue, Z., et al., 2016. Accelerated dysbiosis of gut microbiota during aggravation of DSS-induced colitis by a butyrate-producing bacterium. Sci. Rep. 6 (1), 1–11.

Zhao, X., Ze, Y., Gao, G., Sang, X., Li, B., Gui, S., et al., 2013. Nanosized TiO2-induced reproductive system dysfunction and its mechanism in female mice. PLoS One 8 (4), e59378.

Zhu, Y., Abdullah, L.H., Doyle, S.P., Nguyen, K., Ribeiro, C.M., Vasquez, P.A., et al., 2015. Baseline goblet cell mucin secretion in the airways exceeds stimulated secretion over extended time periods, and is sensitive to shear stress and intracellular mucin stores. PLoS One 10 (5), e0127267.